Journal of Molecular Liquids 350 (2022) 118483

Contents lists available at ScienceDirect

Journal of Molecular Liquids

journal homepage: www.elsevier.com/locate/molliq

On the physical properties of mixtures of nitrate salts and protic ionic liquids

Pablo Vallet [a], Silvia Bouzón-Capelo [a], Trinidad Méndez-Morales [a], Víctor Gómez-González [a], Yago Arosa [a], Raúl de la Fuente [a], Elena López-Lago [a], Julio R. Rodríguez [a], Luis J. Gallego [a], Juan J. Parajó [a,b], Josefa Salgado [a], Mireille Turmine [c], Luisa Segade [d], Oscar Cabeza [d], Luis M. Varela [a,*]

[a] Grupo de Nanomateriais, Fotónica e Materia Branda, Departamento de Física de Partículas y Departamento de Física Aplicada, Facultade de Física and Instituto de Materiais (iMATUS), Universidade de Santiago de Compostela, Campus Vida s/n, E-15782 Santiago de Compostela, Spain
[b] Departamento de Química e Bioquímica, CIQUP-Centro de Investigaçao em Química da Universidade do Porto, Universidade do Porto, P-4169-007 Porto, Portugal
[c] Sorbonne Université, CNRS, Laboratoire de Réactivité de Surface, UMR 7197, 4 Place Jussieu, F-75005 Paris, France
[d] Facultade de Ciencias, Universidade da Coruña, Campus A Zapateira s/n, E-15071 A Coruña, Spain

ARTICLE INFO

Article history:
Received 19 September 2021
Revised 30 December 2021
Accepted 5 January 2022
Available online 19 January 2022

Keywords:
Protic ionic liquids
Inorganic salts
Mixtures
Physicochemical properties
Optical properties
MD simulations

ABSTRACT

We report a systematic study of the effect of salt concentration and its cation valence on several equilibrium and transport properties of mixtures of the model protic ionic liquid ethylammonium nitrate with monovalent ($LiNO_3$), divalent ($Mg(NO_3)_2$ and $Ca(NO_3)_2$), and trivalent ($Al(NO_3)_3$) salts. These properties, determined by appropriate experimental techniques, include density, sound velocity, refractive index, surface tension, conductivity and viscosity. Single-particle dynamics and radial distribution functions were also analyzed by means of molecular dynamics simulations. The temperature dependence of the conductivity was studied in the Vogel-Fulcher-Tammann framework, and we obtained effective activation energies, fragility indexes, and Vogel temperatures. In addition, we performed a high-temperature Arrhenius analysis and we calculated the activation energies of both conductivity and viscosity. Finally, the exponents of the fractional Walden rule for the different mixtures were obtained and the ionicities and fragilities of the systems were analyzed, proving that all the mixtures are subionic and fragile. The distortion of the network of hydrogen bonds characteristic of protic ionic liquids and the formation of long-lived anionic aggregates composed of the cations of the added salt and the nitrate anions in their first solvation shell were found to have a deep impact on the analyzed properties. The role of the surface charge density of the salt cations on the structure and transport properties of the solutions is detailedly analyzed and related to solvation of salt species in the polar nanoregions of the ionic liquid (nanostructured solvation).

1. Introduction

Ionic liquids (ILs) are a new class of amphiphilically nanostructured solvents composed entirely of ions and with melting points usually below 100 °C whose relevance has exponentially increased over the last decades due to a number of unique properties, such as negligible vapor pressure, good thermal and chemical stability, large electrochemical windows and high solvation capacity, arising from a complex interplay of coulombic, hydrogen bonding, and van der Waals interactions of their ions [1]. Regarded as environmentally friendly designer-solvents [2], these liquids are replacing traditional solvents in a surprisingly large number of applications, including electrochemistry, spectroscopy, catalysis and material science to mention a few [3–6].

According to their chemical synthesis, ILs may be broadly separated into two categories: protic ionic liquids (PILs) and aprotic ionic liquids (AILs), the former being formed by the transfer of a proton between a Brönsted acid and a Brönsted base [7–9]. The presence of proton-donor and proton-acceptor sites leads to the formation of a well-known network of hydrogen bonds, which provides them with a number of unique properties compared to other ILs. Ethylammonium nitrate (EAN), reported in 1914 by Walden with a melting point of 287.6 K [10], became the very first known IL. However, although EAN has been widely studied over the last century mainly due to its similarities with water [11], the truth is that AILs have received far more attention than PILs and some

* Corresponding author.
E-mail address: luismiguel.varela@usc.es (L.M. Varela).

https://doi.org/10.1016/j.molliq.2022.118483
0167-7322/

relevant issues on the latter still have not been addressed. Particularly in the field of electrochemistry, PILs have been considered as interesting candidates for fuel cells [12,13] and supercapacitors [14–16]. However, the vast majority of the studies concerning the use of ILs in lithium-ion batteries involved AILs [17–19]. In this regard, several publications reported the potential use of PILs as electrolytes for these devices, since they not only display promising performance but they are also cheaper and easier to synthesize than AILs [20–26]. For example, Menne et al. [20] experimentally investigated for the first time electrolytes composed of a solution containing triethylammonium bis(trifluoromethylsulfonyl) imide (tEATFSI) mixed with lithium bis(trifluoromethylsulfonyl) imide (LiTFSI), and they found that PILs could be successfully introduced in lithium-ion batteries due to their conductivities, capacities and electrochemical windows comparable to those of AILs. A year later [21], they expanded their study reporting an experimental investigation on the lithium coordination in two PILs in order to get a detailed knowledge of the mobility of lithium cations in this kind of electrolytes. The authors obtained a sort of competitive behaviour for the coordination of the IL anion with both positively charged ions; whereas several computational studies [22,23] revealed strong interactions between lithium cations and nitrate anions giving rise to solid-like structures in the polar nanoregions of EAN, PAN and BAN with $LiNO_3$. Moreover, Gómez-González et al. pioneeringly reported similar behavior for divalent salts in mixtures of $Mg(NO_3)_2$ with EAN [27]. In addition, Vogl et al. [25,26] analyzed the conductivity, viscosity and self-diffusion coefficients of pyrrolidinium-TFSI PILs doped with LiTFSI and studied the differences between PILs and AILs in terms of $TFSI^-$ anions coordination to Li^+ cations. This has been recently complemented by Ray et al. [28], who performed a molecular dynamics (MD) study of the solvation of the Li^+ ions in ILs and their influence on their physicochemical properties, proving, as had been previously found by some of us [22,23,27,29,30], that the solvation of the salt cations takes place by "an inhomogeneous structuring mechanism considered to be a "universal" type of ion solvation". This solvation, previously named "nanostructured solvation" by Russina et al. [30], consists in the formation of long-lived, solid-like $[LiA_n]^{1-n}$ clusters in the polar nanoregions of the solvent, preserving, to a great extent, the structure of the IL itself, which is barely affected by the addition of the salt. MD studies with similar results have been reported recently for divalent cations Mg^{2+} and Ca^{2+} in both protic and aprotic environments [27].

On the other hand, several strategies have been followed during the last years with the aim of improving the electrochemical performance of these IL-based electrolytes, ranging from employing mixtures of ILs and organic solvents to doping the ILs with divalent salts [27,31]. As an example, Hayes et al. [31] investigated the bulk nanostructure of several inorganic salt solutions in EAN and ethanolammonium nitrate (EtAN) by means of neutron diffraction and empirical potential structure refinement modelling. They reported the solvation of inorganic salt ions in the polar nanodomains of the mixture, in agreement with the MD results found by some of us [22,23]. Very recently, Russina et al. [30] performed X-ray diffraction and reverse Monte Carlo simulations of the structural properties of a mixture of EAN and $LiNO_3$, showing that lithium cations are distributed in the amphiphilically driven polar domains where they undergo a further level of self-segregation giving rise to ionic clusters. These features constitute the essentials of a new selective solvation mechanism of solutes in amphiphilically nanostructured ionic liquids, and have been also experimentally shown among others by Niedzicki et al. [32], who reported the formation of crystalline complexes where lithium cations and imidazolium anions create chain-shaped $[Li(TDI)_2]_n^{n-}$ polyanions surrounded by $[XMIm]^+$ cations in 4,5-dicyano-2-(trifluoromethyl) imidazolium) (TDI) anion based systems.

The previously mentioned characteristics of the nanostructured solvation of salts in these densely ionic media, with the formation of a pseudolattice of cation–anion complexes in the polar nanoregions of the IL giving rise to stabilized nanocrystals in solution, usually result in reduced solubility of the salts, increased viscosity and decreased electrical conductivity and transport numbers relative to that of the pure IL. This has lead to the consideration of ternary systems in which a molecular cosolvent is added to dilute the mixture, restoring its above mentioned properties to battery-grade values. For instance, Karpierz et al. [33] combined glymes at appropriate concentrations to optimize electrical conductivity and lithium cation transference numbers profiting from the formation of $[Li(glyme)_n]^+$ complexes in the mixture together with immobile aggregated lithium polyanions responsible for higher transference numbers. On the other hand, MD simulations of N-methyl-N-propylpyrrolidinium bis(trifluoromethanesulfonyl) imide (TFSI) ionic liquid [Pyr13][TFSI] doped with [Li][TFSI] salt mixed with the organic solvents ethylcarbonate and acetonitrile were reported by Li et al. [34], and they found enhanced the ion mobility, specially that of the Li^+ cation. The transport number of the salt cation doubles at 40 mol % of acetonitrile, and its residence time in the cages of the ILs is dramatically reduced in the ternary mixtures. Of course, this strategy of enhancing the IL-salt mixture properties with molecular cosolvents should also take into account the decrease in electrochemical stability resulting from the introduction of the cosolvent. For that, and despite the very large decrease of viscosity and increase of electrical conductivity [35], usually water has been avoided due to its evident inconveniences, but recently the "water-in-salt" electrolytes have been shown to be compatible with high-voltage aqueous lithium ion batteries [36]. In highly concentrated ionic solution, mixed metal/water/anion complexes are formed, so water molecules are mainly in their hydrated form, leading to enhanced electrochemical window. Hence, the possibility of preparing water-IL-salt ternary mixtures, quite natural due to the composition of hydrated salts, arises and the properties of these mixtures must be conveniently explored.

On the other hand, although lithium is the most successful material for batteries so far, the increasing interest in electrochemical devices has led to the need of developing batteries with progressively better performance. Hence, divalent and trivalent salts have been considered and they also showed prosperous operation and several advantages [37,38]. In a recent paper [27], Gómez-González et al. compared the structure and single-particle dynamics of EAN doped with divalent salts with those of an AIL, 1-butyl-3-methylimidazolium hexaflurophosphate ($[BMIM][PF_6]$), mixed with the same inorganic salts. Their MD simulations indicated stronger electrostatic correlations of the polar nanoregions in the mixtures with divalent salts when compared to those with monovalent cations. However, a further understanding of the effect of adding inorganic salts to ILs is still required. Specifically, the knowledge of the physical properties of solutions of multivalent salts in PILs is still in its infancy.

In this work we deepen into the physical effects of salt solution in ILs reporting experimental measurements and MD simulations of several thermodynamic and transport properties of monovalent ($LiNO_3$), divalent ($Mg(NO_3)_2$, $Ca(NO_3)_2$) and trivalent ($Al(NO_3)_3$) salts with common anion dissolved in EAN. In order to understand the effect of the nanostructured solvation of ions in dense ionic solvents, we analyze the dependence of these properties on the salt concentration as well as on the charge of their cations. Particularly, we report measurements of volumetric properties, refractive indices, surface tension, electrical conductivities, and viscosities. Moreover, we analyze fragilities and ionicities of the investigated mixtures from the fragility and Walden plots, respectively. To the best of our knowledge, this is the first time most of them are reported for PILs doped with inorganic salts.

The structure of the paper is as follows. In the next section we describe the experimental and computational techniques used to determine the properties of the systems investigated. The following section includes the discussion of the results and, finally, we summarize our main conclusions.

2. Experimental and computational details

2.1. Chemicals

EAN was purchased from IOLITEC with a purity degree $> 97\%$, and it was used as received. We prepared solutions of EAN with different salts: $LiNO_3$ (Merck, 99.995%), $Ca(NO_3)_2{\cdot}4H_2O$ (Panreac, 98.0–103.0%), $Mg(NO_3)_2{\cdot}6H_2O$ (Panreac, 98.0–102.0%) and $Al(NO_3)_3{\cdot}9H_2O$ (Scharlau, 98–192%) and concentrations up to the saturation limits (see Table 1). The purities of the divalent and trivalent salts refer to contents measured by the complexometric titration method.

The solubilities of the salts in EAN were determined gradually adding small amounts of the salt to 5 g of EAN -taking into account their hydration degrees to calculate the concentrations EAN samples- and drying the mixture at 333 K under continuous sonication and moderate vacuum ($P \leqslant 10^{-3}$ atm) during $48 - 72$ hours, and the occurrence of any precipitate (usually formed between $24 - 48$ hours after mixing) was visually checked.

The residual amount of water was then tested for the saturated mixtures by means of a Karl Fischer analysis using a Mettler Toledo Coulometer and by nuclear magnetic resonance (NMR) measurements. ^{1}H NMR spectra were obtained using a Varian Inova 750 spectrometer at 750 MHz without rotation of the samples and without using any internal or external standards.The chemical shift (δ) of a line was measured from the position of the line ♯1 for which the δ value was taken as 1.0 ppm according to available literature data [39]. NMR measurements indicate that water molecules are free in the bulk of mixtures with cations of low surface charge density, Li^+ and Ca^{2+}, showing chemical shifts $\delta = 4.7$ ppm in both cases, while they are hydrating the highly charged ones, Mg^{2+} ($\delta = 6.5$ ppm) and Al^{3+} ($\delta = 9$ ppm), with no free water detected in these latter samples after drying. According to our observations, some water content (albeit residual) seems to be necessary for achieving the dissolution of the salts in the dense ionic environments up to these relatively high solubility limits, since almost no solubility was detected if mixtures were prepared after drying EAN and the salt. Moreover, as we will describe in more detail later, this bounded water could be not a major drawback in what electrochemical window is concerned. The actual average water contents of our saturated samples are shown in Table 1.

2.2. Density and ultrasound velocity measurements

Density and speed of sound were continuously, simultaneously, and automatically measured for a temperature interval from 288 K to 313 K using a DSA 5000 Anton Paar SVM 3000 density and sound velocity analyzer. The densimeter was calibrated with dry air and distilled water at known pressure and temperature. This apparatus is equipped with a latest-generation vibrating tube for density measurements and a stainless-steel cell connected to a sound velocity analyzer with resolutions of $\pm 10^{-6}$ g · cm^{-3} and 10^{-2} m · s^{-1}, respectively. Both the speed of sound and density are extremely sensitive to temperature, so the latter was controlled to within $\pm 10^{-3}$ K by means of a Peltier module. The reproducibility of density and ultrasound measurements was $\pm 10^{-5}$ g · cm^{-3} and 10^{-1} m · s^{-1}, respectively.

2.3. Surface tension measurements

Surface tension measurements in the temperature range from 283.15 to 313.15 K were made by two methods to ensure reproducibility. First, we employed a pendant drop shape method, whose specific details have been reported elsewhere [41]. This equipment is managed by a Windows integrated program (DINATEN) that provides the interfacial. Moreover, we used a Krüss tensiometer (K11 model) based on the Wilhelmy plate method. The solutions were maintained at a constant temperature (±0.1 °C) in a circulating water bath.

2.4. Viscosity and electrical conductivity measurements

Viscosity measurements were obtained by means of an Anton Paar automatic microviscosimeter in a temperature interval from 288.15 to 313.15 K, controlled automatically by the equipment. We employed two measuring system sets: the first one equipped with a capillary tube of diameter 1.8 mm and a ball of diameter 1.5 mm was used to obtain viscosities up to 70 mPa · s^{-1}, and the second one, with diameters of 4.0 and 3.0 mm, respectively, for higher viscosities.

Electrical conductivity was measured at a constant frequency of 500 Hz using a conductimeter Mettler Toledo, model Sevenmulti S47 with an Inlab 730 conductivity probe operating over a wide temperature range from 223 to 373 K. The integrated temperature sensor avoids the need for a separate temperature probe when compensating for the difference in temperature between the sample and the reference temperature. The temperature of the samples (between 283 and 373 K) was controlled using a Julabo F25 thermostat calibrated with an external sensor Crison T-637, which provided a precision better than 0.1 K in the range of temperature measured. It is important to note that all measurements were done by means of a static isothermal method; thus, the sample was allowed to spend about 15 min at constant temperature before any single measurement was performed, while close to solid–liquid phase transitions that period was increased to at least 30 min. For low temperatures (< 258 K), temperature control was achieved by means of a Lauda Proline RP 890 with a measurement range that extends from 178 to 473 K.

Table 1
Solubility limits of salts in EAN at room temperature at the shown average water contents of the mixtures, most reliable ionic radii in the coordination number shown in brackets, ionic potentials (q/r) and surface charge densities ($q/4\pi r^2$) of the salt cation for $LiNO_3$, $Mg(NO_3)_2$, $Ca(NO_3)_2$ and $Al(NO_3)_3$. Ionic radii were taken from Ref. [40] for the used oxidation states. ($*$) indicates hydration water. Uncertainty for the solubility is 0.1 mol kg^{-1}.

Salt	Solubility ($mol{\cdot}kg^{-1}$)	Water content (ppm)	*Ionic radius* (*Å*)	*Ionic potential* ($e\ nm^{-1}$)	*Charge density* ($e\ nm^{-2}$)
$LiNO_3$	2.4	< 100	0.59 (IV)	16.9	22.9
$Ca(NO_3)_2$	1.0	< 100	1.0 (VI)	20.0	15.9
$Mg(NO_3)_2$	2.5	$< 10000^{(*)}$	0.72 (VI)	27.8	30.7
$Al(NO_3)_3$	2.5	$< 10000^{(*)}$	0.54 (VI)	55.6	81.9

2.5. Refractive index

The wavelength-dependent refractive index was measured by a white light spectral interferometry-based technique named RISBI (Refractive Index Spectroscopy by Broadband Spectroscopy) [42]. The experimental device is constituted by a homemade instrument that is composed by a stabilized halogen light source, a Michelson interferometer and a fiber coupled spectrometer covering the wavelength range from 400 to 1000 nm. The instrument has already been exhaustively described in previous publications [42–44]. Refractive index at 589 nm was also measured by Abbe Refractometry by means of a multi-wavelength refractometer (Atago DR-M2) with a measurement range from 1.30 to 1.71 at this wavelength. The temperature was controlled by using a circulating water bath and measured with a resolution of 0.1 K by means of a thermocouple sensor in direct contact with the IL. The experimental resolution of these devices is 2×10^{-4}.

2.6. Simulation details

MD simulations of pure EAN mixed with a 10% mole percentage of $LiNO_3$, $Mg(NO_3)_2$ and $Ca(NO_3)_2$ at $T = 298.15$ K and $P = 1$ atm were carried out using the GROMACS 4.5.4 package [45]. With regard to the parametrization of the ions, the OPLS-AA force field was used, which is an all-atom version of the OPLS force field that models every hydrogen atom bonded to carbon explicitly and whose details have been reported in Ref. [46].

The ethylammonium cation was modelled by using the Lennard-Jones (LJ) parameters previously reported by Umebayashi et al. [47], while its partial charges were evaluated by Choe et al. [48] using the 6-31G** method. Lithium cations were modelled as single sites of charge +1, whereas magnesium and calcium cations were modelled by a single site of charge + 2; their LJ parameters were directly taken from GROMACS database. On the other hand, each nitrate anion was parameterized as a set of seven sites, three of them heavy and the other four virtual. A heavy site carries no charge, but it is associated with 1/3 of the total mass of the ion and placed so as to yield the right tensor of inertia. In contrast, virtual sites are massless but have partial charges of $q_N = +0.794$ for the nitrogen atom and $q_O = -0.598$ for the oxygen atoms [49], whose LJ parameters are, respectively, $\sigma_N = 3.496\cdot10^{-1}$ nm, $\varepsilon_N = 7.1128\cdot10^{-1}$ kJ mol^{-1}, $\sigma_O = 3.175\cdot10^{-1}$ nm, and $\varepsilon_O = 8.7864\cdot10^{-1}$ kJmol^{-1}; and were fitted in order to reproduce the experimental density of the pure IL.

The initial configuration for the percentage of salt used in the calculations, which is a lower value than the solubility limit in all cases, was obtained by randomly inserting 450 ionic pairs of IL in a cubic box. The number of salt molecules was calculated for each situation by considering each ionic pair as a single unit in the calculation of mole fraction and it was chosen to guarantee statistical significance of the results ($N > 50$ ion pairs). The rest of the details of the simulations have been reported elsewhere [22,27].

For each molar percentage of salt, the system was equilibrated for 20 ns in the isothermal-isobaric (NpT) ensemble applying periodic boundary conditions. We have employed 20 ns long simulations, time enough to ensure complete equilibration and sampling of relevant enough regions of the phase space. One must recall to this respect that the experimental bulk density of the IL and its mixtures is reached after 0.5 ns, and the correlation of the ion velocities are completely dumped out after 1 ns. Then, the results of an additional 10 ns–long simulation in the isothermal-isobaric ensemble were used for the analysis of the structure of the mixtures.

3. Results and discussion

Firstly, we measured the solubility limits of the different salts in EAN at room temperature according to the procedure described above, and the results are shown in Table 1. As can be seen there, the salts with the lowest solubilities are those containing less densely charged cations. We must mention that these systems must be considered as ternary systems, since they include different amounts of water (see Table 1). Notwithstanding, these quantities are low enough to be considerably below the "solvation numbers" of conventional electrolytes ($\sim$ 1.0 mol·kg^{-1}). As the number of salt + IL ions largely outnumber that of solvent molecules (water), these systems fit the definition of water-in-salt electrolytes of Suo et al. [36]. As reported by the authors, the scarcity of water molecules in highly concentrated electrolytes solutions (at molal concentrations $>$ 10 m) leads to drastic changes in the solvation sheath of the salt cations, since mixed complexes of cation–anion and water molecules are formed. It is this inclusion of the IL and salt anions in the solvation shell of the cations which alters the interfacial chemistry at the electrodes, realizing much expanded electrochemical window [36]. Expectedly, this is also the case in our systems. For example, in the case of the lithiated mixtures, *ab initio* MD simulations [50] showed that lithium ions have a well-defined first hydration shell of four water molecules arranged with tetrahedral symmetry in dilute enough aqueous electrolyte solutions. Each of these first-shell hydration molecules are bonded to three other water molecules in the second hydration shell, and their fourth binding is occupied by the central lithium ion itself. However, in our dried saturated EAN/$LiNO_3$ mixtures (100 ppm water content), only 3 water molecules per 1000 Li cations are available. Hence, considering that completely dried samples are immiscible, we conclude that the solvation shells of Li cations include these residual water together with NO_3^- anions. A detailed investigation of the electrochemical windows and interfacial chemistry of these ternary mixtures of ILs, salts and residual water is, however, needed to confirm these claims, and systematic work is now in progress.

In order to understand the solubility trend (Ca<Li≈Mg = Al), we must consider the peculiar nanostructured solvation mechanisms of ions in ILs. As we described in the Introduction to this paper, the added ions are known to be transferred to the polar nanocavities in the bulk mixtures [22,30], while the structure of the polar nanodomains of the IL is highly resilient to salt addition [22,27]. Only the heights of the peaks of the radial distribution functions (RDFs) are slightly changed as concentration increases, and no relative shift of their positions is detected. Hence, no significant effect is exerted by the salt cations in the structure of the liquid beyond some gradual transference of $[NO_3]^-$ to the interior of the polar regions from the $[NH_3]^+$ neighborhood. The insertion of a cation in these regions of the IL produces strongly bound cation–anion complexes $[XA_n]^{n-1}$ with intense electrostriction of the polar regions. These complexes are more strongly bound the higher the surface charge density of the cation. Besides, highly charged cations like Mg^{2+} or Al^{3+} should induce nitrates to coordinate those regions with the highest negative charge density, i.e. the oxygens in the IL anion. This coordination gives rise to a very strong solvation of the salt cations, which could prevent crystallization more efficiently, incrementing the solubility limit of the salt. On the other hand, the cations with the lowest charge density would produce more weakly bound complexes and, therefore, they allow an easier formation of crystallization nuclei (probably, mixed water-anion-metal cation $[M(H_2O)_n(NO_3)_m]^{z-m}$ complexes) in the polar domains that actually lead to precipitation of the solid salt at lower concentrations. Moreover, as we previously mentioned, these com-

plexes are probably further stabilized by the presence of water molecules in the first solvation shell of the anions.

This coordination between nitrate anions and salt cations can be clearly observed by quantifying spatial structure through the analysis of the RDF,

$$g_{ij}(r_{12}) = \frac{1}{\rho_i \rho_j} \sum_{i,j}^{N} \left\langle \delta\left(\vec{r}_1 - \vec{r}_i\right) \delta\left(\vec{r}_2 - \vec{r}_j\right) \right\rangle, \quad (1)$$

where ρ is the number density, N stands for the number of particles in the system, i and j run over all the species, and brackets indicate the ensemble average. The accuracy of the OPLS-AA force field was previously tested comparing the experimental density of the mixtures to the MD predictions [27]. The RDFs involving the nitrate anions and the salt cations for a salt fraction of $x_{salt} = 0.1$ in their corresponding mixtures are shown in Fig. 1. It must be clarified that for the calculations of the RDFs we considered the center of mass of the defined groups. As it was previously stated, this figure indicates a stronger interaction between $[NO_3]^-$ anions and the corresponding salt cations the greater the charge density of the salt, which contributes to the formation of stable anion-cation clusters and their slower diffusion. In addition, the increase of the charge density of the salt cations (see Table 1) leads to the virtual disappearance of the first part of the double peak corresponding to the bidendate conformation, and to a strong preference for a monodentate coordination with the negatively charged oxygens of the nitrate anion, as mentioned previously. This could possibly prevent the efficient packing of the highly charged cations in the nanoregions, hence leading to enhanced solubilities [27]. However, we should also take into account that the actual mixtures of Mg^{2+} and Al^{3+} employed in this study contain also hydration water (not explicitly included in the simulations, since it presumable leads only to minor modifications of the overall structure of the system).

The RDFs provide a structural picture of the local environment of the cations in which the first shells of cations with the lowest valency are split into two subshells. The first shell of the salt cations in the studied non hydrated mixtures consists of 4 ($LiNO_3$) and 6 ($Mg(NO_3)_2$, $Ca(NO_3)_2$, and $Al(NO_3)_3$) NO_3^- anions coordinating the corresponding salt cation. In the case of cations with low ionic potentials and charge densities (Li and Ca), these anions are placed

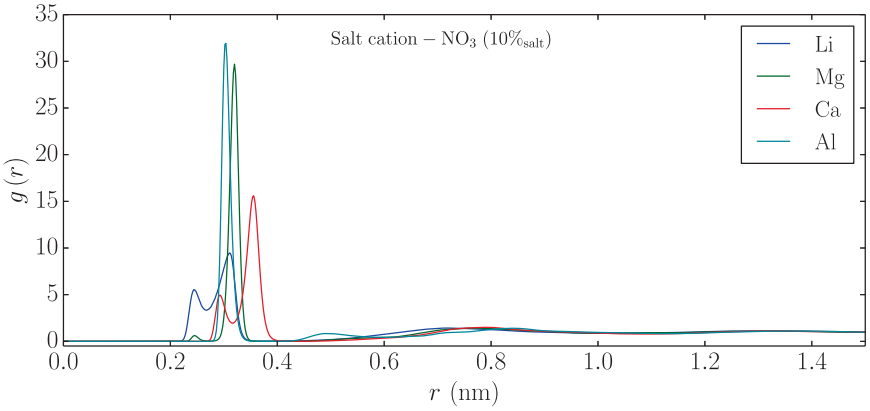

Fig. 1. Anion-salt cation RDFs in mixtures of EAN with $LiNO_3$, $Mg(NO_3)_2$, $Ca(NO_3)_2$ and $Al(NO_3)_3$ for a salt concentration of $x_{salt} = 0.1$.

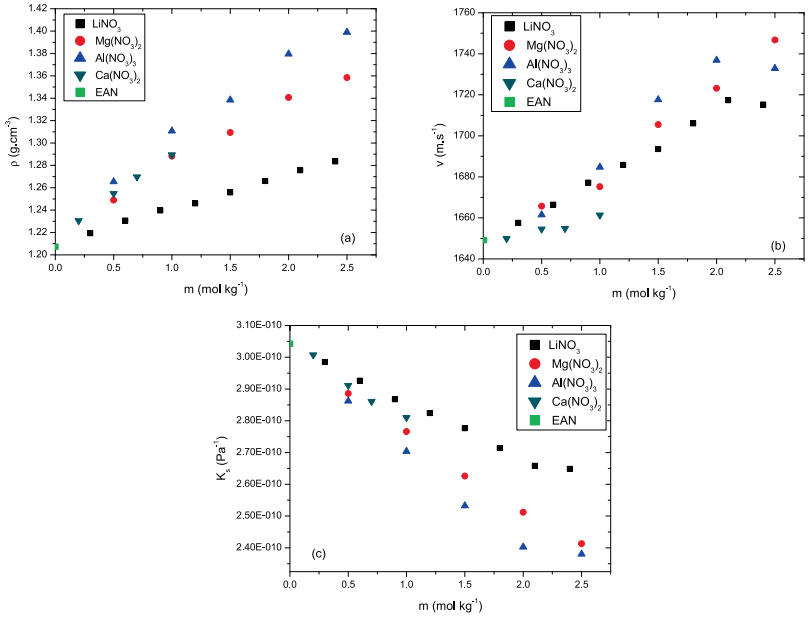

Fig. 2. Concentration dependence (molality) of the density (a), the speed of sound (b) and the adiabatic compressibility (c) of pure EAN and its mixtures with $LiNO_3$, $Mg(NO_3)_2$, $Ca(NO_3)_2$ and $Al(NO_3)_3$ at 298.15 K. Supersaturated values are shown for Li, Mg and Al mixtures.

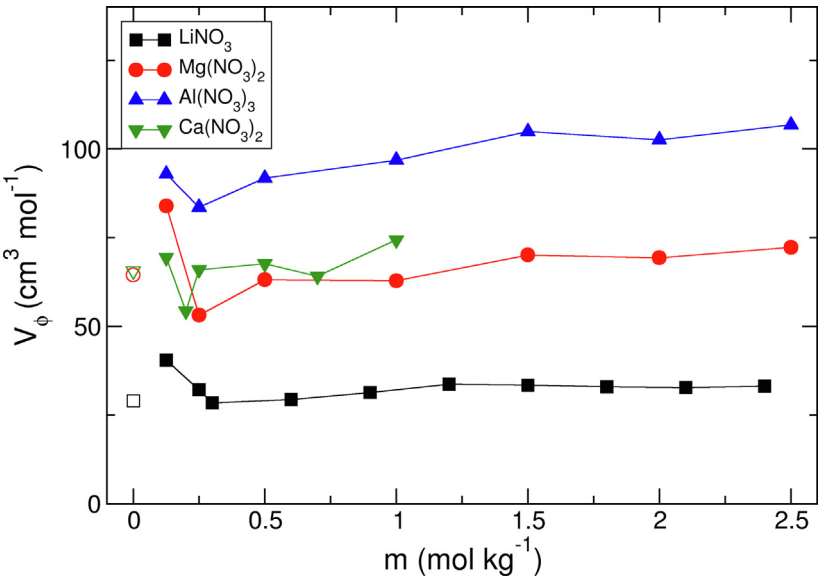

Fig. 3. Concentration dependence of the apparent molar volume of $LiNO_3$, $Mg(NO_3)_2$, $Ca(NO_3)_2$ and $Al(NO_3)_3$ in mixtures with EAN. The open dots correspond to the values for the pure anhydrous salts [51]. The density of anhydrous $Al(NO_3)_3$was not available.

at two different distances corresponding to monodentate and bidentate conformations, in the latter with slightly higher probability the lower the size and the rest at ca. 0.5 nm [27]. However, the bidentate (lower distance) coordination mode is almost completely absent in the case of mixtures of EAN and Mg^{2+} and it does not appear at all in the case of Al^{3+}, which confirms the role of the charge density in the solvation of these cations in the polar nanoregions of the IL in the form of ionic clusters $[XA_n]^{1-n}$. Of course, the composition of these simulated clusters could change if water was included in the simulations, a work which is now in progress.

Fig. 2 shows the concentration dependence of the speed of sound, v, in the hereby reported systems (b) together with the adiabatic compressibility of these mixtures (c) obtained by means of the well-known Laplace equation, $K_s = 1/\rho v^2$. The inverse relation of this magnitude with the structural order of the mixtures explains the fact that K_s decreases increasing the amount of salt in all the analyzed cases. Furthermore, it can be seen that the adiabatic compressibility decreases with the valency of the salt cation, indicating that the addition of those salts with cations of larger valencies leads to more densely packed and more compact mixtures. This effect is more pronounced the larger the valency, and comes from the formation of compact ionic clusters. Moreover, as it was previously reported by some of us [27], the network of directed hydrogen bonds in EAN is more strongly distorted the greater the charge density of the salt cations, which leads to a stronger molecular reorientation that breaks the liquid network of hydrogen bonds inducing a structural transition in the mixture that makes it more difficult to be compressed.

Further information on the structural effect of salt addition to EAN can be obtained with volumetric studies of the solutions. Fig. 2 (a) shows the concentration dependence of the density (ρ) of pure EAN and its mixtures with $LiNO_3$, $Mg(NO_3)_2$, $Ca(NO_3)_2$ and $Al(NO_3)_3$ at room temperature. A monotonic increase with concentration is registered for all the studied mixtures, which is approximately linear except at concentrations close to saturation. In addition, the density increases at constant concentration as the mass and the charge of the salt cation increase. In the case of divalent salts, those mixtures with Ca^{2+} show approximately the same densities as those with Mg^{2+} within our experimental resolution.

Moreover, some of us have recently reported MD simulations proving that both the apparent molar volumes and the partial molar volumes for the salts with monovalent and divalent cations remain approximately constant upon the addition of salt [27]. This behavior suggests that the local environment of the salt ions changes very little with concentration in EAN, and the experimental results obtained in this paper are in very good agreement with these predictions (see Fig. 3). As can be also seen there, these

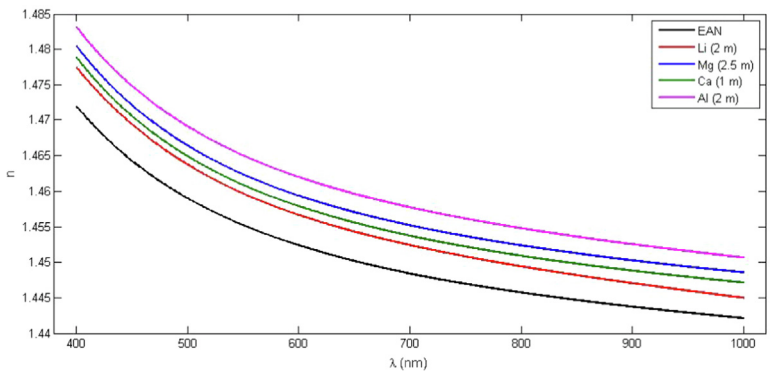

Fig. 4. Wavelength dependence of the refractive index of pure EAN and its mixtures with $LiNO_3$, $Ca(NO_3)_2$, $Mg(NO_3)_2$ and $Al(NO_3)_3$ near the solubility limit.

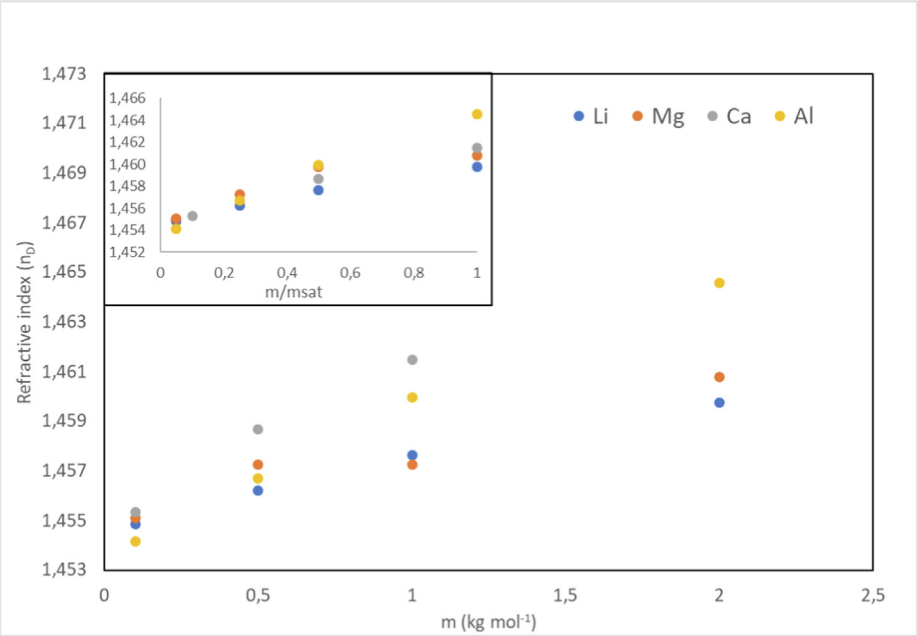

Fig. 5. Concentration dependence of the refractive index of the mixtures of EAN with $LiNO_3$, $Ca(NO_3)_2$, $Mg(NO_3)_2$ and $Al(NO_3)_3$ for $\lambda = 589$ nm and $T = 298.15$ K. The inset shows the same values plotted against the concentration normalized by the solubility limits.

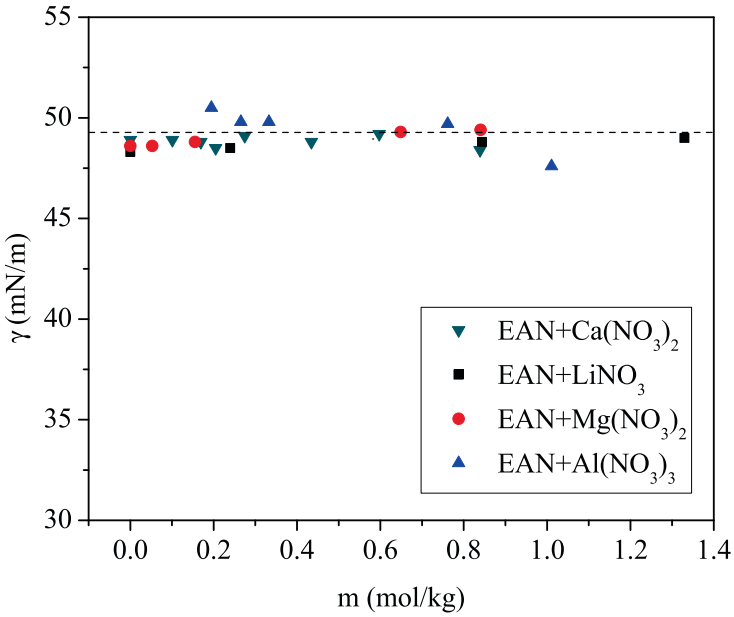

Fig. 6. Concentration dependence (molality) of the surface tension of mixtures of EAN with $LiNO_3$, $Mg(NO_3)_2$, $Ca(NO_3)_2$ and $Al(NO_3)_3$ at 298.15 K. Dashed line corresponds to the value of pure EAN (49.350 mN m^{-1}) reported in Ref. [53].

values at high concentrations differ relatively few from those for the pure salts, indicating that the salts are accommodated in a solid-like fashion in the polar nanoregions of the IL. At low concentrations we can observe slight increases in all the apparent volumes due to concentration uncertainties. Probably, these volumes correspond to regions with relatively isolated ions within the polar nanoregions, that tend to develop into quasisolid phases at high concentrations.

Trying to get a further confirmation of the formation of these solid-like structures in the mixtures upon salt addition, we measured the refractive index dispersion of the different samples and also their dependence on salt concentration. Our results are plotted in Fig. 4 for the studied mixtures. All the mixtures show normal dispersion as it was expected since neither the PIL nor the salts presented anomalous dispersion or electronic resonances in this spectral range. By comparing with the pure PIL wavelength dependent refractive index, the effect of the addition of the salt in the refractive index is similar all over the spectral range considering the experimental uncertainty. The effect increases with the valence of the metal, and it is attributed to changes in density

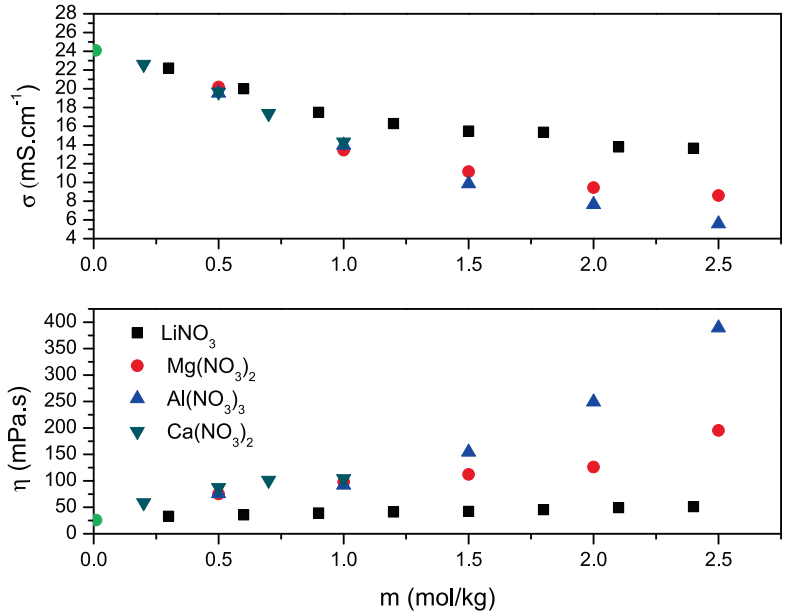

Fig. 7. Concentration dependence of the conductivity (a) and the viscosity (b) for pure EAN and its mixtures with $LiNO_3$, $Mg(NO_3)_2$, $Ca(NO_3)_2$ and $Al(NO_3)_3$ at 298.15 K. Green dots correspond to the values of pure EAN (data taken from Ref. [53]).

and in polarizability. The latter are mainly conditioned by the valence of the metals, or number of nitrate groups, and the former by the refractive index of the salts.

The concentration dependence of the refractive index of the studied mixtures is shown in Fig. 5. Notice, firstly, that the refractive indices of saturated solutions of divalent salts (1 mol·kg^{-1} Ca$(NO_3)_2$ and 2 mol·kg^{-1} $Mg(NO_3)_2$) are very close, with differences between them below 9×10^{-4}. This can be understood by considering that although the density of $Ca(NO_3)_2$-PIL solution (1.29 g·cm^{-3}) is smaller than that of the $Mg(NO_3)_2$-PIL solution (1.36 g/cm^3), the refractive index of $Ca(NO_3)_2$ (n_D= 1.46) is higher than the refractive index of $Mg(NO_3)_2$ (n_D=1.34), respectively, and both contributions offset each other. The influence of polarizability can be behind the value of refractive index of the monovalent $LiNO_3$-PIL dissolution (n_D=1.4597), closer to the refractive index of the saturated divalent solutions than expected. Although the density value is the smallest (1.27 g/cm^3), the refractive index value of the pure salt is the highest (n_D =1.735). The maximum value of the refractive index is found for the 2 mol·kg^{-1} PIL + $Al(NO_3)_3$. The density value is also the highest and the refractive index of $Al(NO_3)_3$ salt is n_D =1.54. However, this reasoning is not sufficient to explain why the refractive index of the Ca-based solution is higher than that of PIL + $LiNO_3$, indicating that other factors associated with the structure of the solvation, such as packing, closely related to the valence, contribute to the final value of the refractive index.

As can be also seen in Fig. 5, the refractive indices of the studied solutions increase with salt concentration until saturation. The behaviour observed in the mixtures is compatible with more solid-like, less compressible mixtures if one takes into account that the refractive index is influenced by density fluctuations, and that the magnitude of these fluctuations is roughly proportional to the glass transition temperature and the compressibility of the melt above the glass transformation temperature [52]. The observed trend is compatible with this rule. Besides, as can also be seen in Fig. 5, a sort of corresponding states trend is registered for Ca^{2+} and Mg^{2+}, which behave closely alike at the same reduced density. Specifically, the exception of Ca^{2+} in the density space disappears in the reduced density plot. This suggests the occurrence of electronically equivalent states in these systems controlled basically by the electronic density spatial distribution, but certainly more work is needed in this line in order to clearly elucidate the origin of this behavior and the role, if any, the metal cation valency could play in it.

Fig. 6 shows the concentration dependence of the surface tension of the systems considered in this study. As one can see in this representation, within the uncertainty of our experimental procedure, only very small variations of the surface tension with salt concentration or with the valence of the salt cation are registered. Hence, just like with that in the bulk mixture, we can conclude that the addition of salt to pure EAN provokes very small changes on the surface environment suggesting also a relative indifference of salt ions either for bulk or surface environments. This may be due to the nanostructure of the PIL allowing an equivalent accommodation of the salt ions at the air–liquid interface and in the bulk. It is well-known [8] that both IL ions are present at the surface, so both cation and anion exert some influence on the surface tension, and the essential details of the nanostructure of the bulk IL are reproduced at the interface, giving rise to a two-dimensional network of polar nanoregions where the salt ions can be solvated in a similar fashion to that in the bulk. According to previously reported models [7,54], the charged groups point towards the bulk of the PIL, and the hydrocarbon chains of the cations are exposed to air, which could provide a rationale for the relative independence of the surface tension of the solutions on ion valence. Besides, a decrease in the hydrogen bonding degree of EAN is known to be associated with the increase of salt concentration both for monovalent [22] and divalent [27] salts, being the effect slightly more marked in the latter case. This decrease would induce a reduction of the energetic requirements for the deformation of the IL–air interface, hence leading to a decrease of the surface tension with salt addition. However, this tendency seems to be compensated by the energetically-favored solvation of the ions in the polar nanoregions of the bulk PIL, so the solvation of salts in this PIL seems to produce little or no effect on the surface tension, behaving very much like sugars in aqueous solutions [55].

Turning now to the effect of salt addition on the transport properties of EAN, Fig. 7 represents the electric conductivity (a) and vis-

cosity (b) measurements for the systems analyzed in this paper at room temperature. The conductivity of these mixtures decreases not only increasing the amount of salt, but also as increasing the salt cation charge, whereas the concentration dependence of the viscosity shows exactly the opposite behaviour. This reflects the slowdown of both the mass and charge transport mechanisms, the more intense the greater the charge density of the added salt cations.

To get a more sound microscopic foundation, in addition to these macroscopic results, single-particle dynamics of the ions in monovalent and divalent salts was analyzed using MD simulations by calculating the mean square displacement (MSD) of salt cations in the mixture, defined as

$$MSD = \left\langle \Delta|\vec{r}(t)|^2 \right\rangle = \frac{1}{N}\left\langle \sum_{i=1}^{N} |\vec{r}_i(t) - \vec{r}_i(0)|^2 \right\rangle, \quad (2)$$

where $\vec{r}(t)$ is the location of the center of mass of ion i at time t, the sum extends over all the ions present in the mixture and brackets indicate the ensemble average. In Fig. 8 we show an illustration of the behaviour of MSDs of lithium, calcium, magnesium and aluminium cations for a salt concentration $x_{salt} = 0.1$ in their corresponding mixtures. The results show a slower diffusion of the ions the larger the valency of the salt cation. This behaviour is consistent with their higher charge densities drastically reducing their mobilities, forcing them to remain in very long-lived cages. As we reported in previous works [29,22], the behaviour of these systems suggests the formation of anionic aggregates (composed of the salt cations and the anions in their first coordination layer) that diffuse as pseudo-stable kinetic entities. The coordination between nitrate anions and the salt cations was found to be stronger the larger the valence of the salt [22,27], which ultimately leads to more resilient clusters and a slower dynamics. However, at long enough times, it seems that Al^{3+} crosses to the diffusive regime faster than Ca^{2+}, which could probably be related with the smaller size of the trivalent cation (see Table 1).

In order to further analyze the dynamics of these systems, we measured the temperature dependence of their electrical conductivity and viscosity. The results for the electrical conductivity

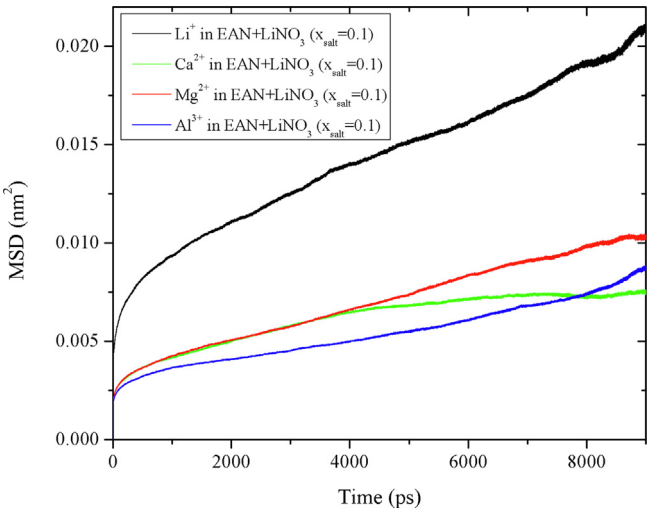

Fig. 8. Time dependence of the MSD of the salt cation in mixtures of EAN with $LiNO_3$, $Mg(NO_3)_2$, $Ca(NO_3)_2$ and $Al(NO_3)_3$ for a salt molar fraction $x_{salt} = 0.1$.

(measured during cooling cycles) saturated solutions and for an intermediate concentration are plotted in Fig. 9.

In this representation we can observe that the conductivities fall significantly below the value of the pure EAN in the liquid phase (both above the melting temperature, 285 K, and in the supercooled region), confirming the effect of salt addition on the electrical conductivity of ILs commented above. Moreover, the conductivities of the salts with the cations of lower charges are consistently larger than those with higher ionic potentials. Moreover, the observed conductivities of the mixtures fall well below the values for the pure IL measured during the cooling part of the freezing-melting hysteresis loops at the liquid–solid phase transition. Besides, no abrupt fall of the electrical conductivity is registered in the supercooled regions of these mixtures, something which was analyzed and attributed to peculiarities of the hydrogen bond network in pure EAN [53]. The role of the cation formal charge on the behaviour of supercooled electrolyte solutions was originally

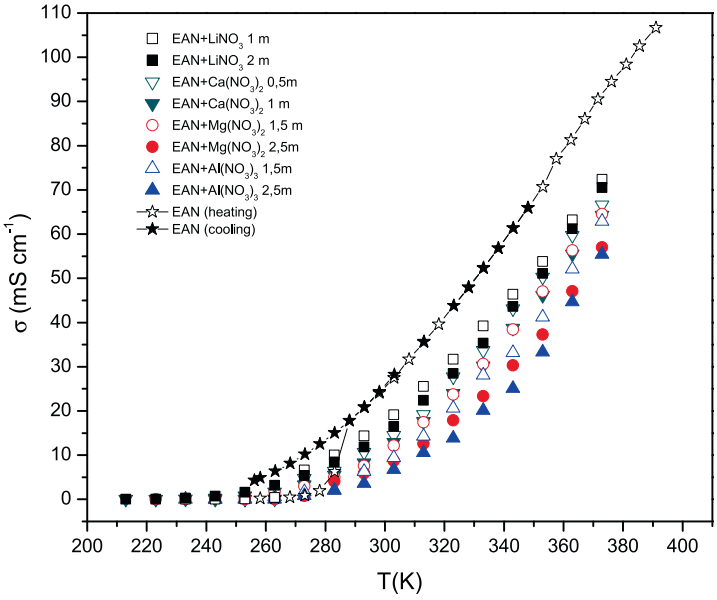

Fig. 9. Temperature dependence of the electrical conductivity of mixtures of EAN and $LiNO_3$, $Mg(NO_3)_2$, $Ca(NO_3)_2$ and $Al(NO_3)_3$ at saturation and an intermediate concentration. Stars correspond to the conductivities of pure EAN during heating (open symbols) and cooling (solid symbols) cycles (see Ref. [53] for details). The solid lines are guides to the eye.

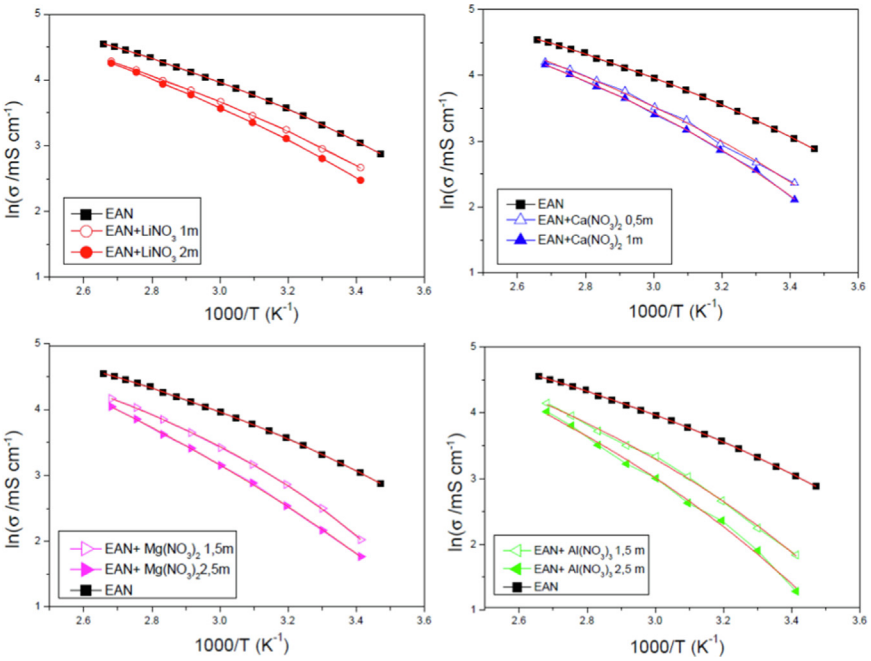

Fig. 10. Arrhenius plots for the conductivities of pure EAN (data taken from Ref. [53]) and its mixtures with $LiNO_3$ (a), $Ca(NO_3)_2$ (b), $Mg(NO_3)_2$ (c) and $Al(NO_3)_3$ (d) near the solubility limit and at an intermediate concentration. The red lines shown in the plot correspond to the fitting to the VFT Eq. 3 (parameters shown in Table 2).

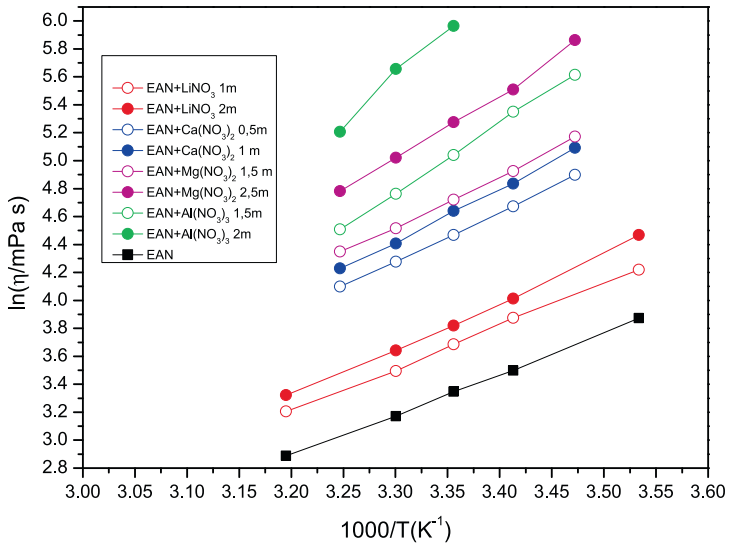

Fig. 11. Arrhenius plots for the viscosities of pure EAN and its mixtures with $LiNO_3$ (a), $Ca(NO_3)_2$ (b), $Mg(NO_3)_2$ (c) and $Al(NO_3)_3$ (d) near the solubility limit and at an intermediate concentration. The lines shown in the plot are guides to the eye.

Table 2
Fitting parameters of the experimental conductivities of mixtures of EAN with $LiNO_3$, $Mg(NO_3)_2$, $Ca(NO_3)_2$ and $Al(NO_3)_3$ to the VFT equation (Eq. 3).

IL	$\ln \sigma_\infty$ *(mS cm^{-1})*	*D*	T_0 *(K)*	*B (kJ mol^{-1})*
EAN	6.781 ± 0.064	2.68 ± 0.17	170.8 ± 3.2	3.81
EAN + $LiNO_3$ (1 m)	6.87 ± 0.17	3.29 ± 0.49	164.0 ± 8.0	4.50
EAN + $LiNO_3$ (2 m)	7.15 ± 0.15	3.74 ± 0.46	162.7 ± 6.6	5.07
EAN + $Ca(NO_3)_2$ (0.5 m)	7.08 ± 0.09	3.3 ± 1.4	173.0 ± 21.0	4.74
EAN + $Ca(NO_3)_2$ (1 m)	6.81 ± 0.18	2.57 ± 0.34	189.1 ± 6.5	4.05
EAN + $Mg(NO_3)_2$ (1.5 m)	6.56 ± 0.08	1.99 ± 0.13	$203,6 \pm 2,3$	3.38
EAN + $Mg(NO_3)_2$ (2.5 m)	8.10 ± 0.23	6.01 ± 0.87	150.0 ± 8.0	7.53
EAN + $Al(NO_3)_3$ (1.5 m)	7.23 ± 0.42	3.16 ± 0.88	185.0 ± 14.0	4.87
EAN + $Al(NO_3)_3$ (2.5 m)	7.75 ± 0.07	4.10 ± 1.75	179.0 ± 22.0	6.11

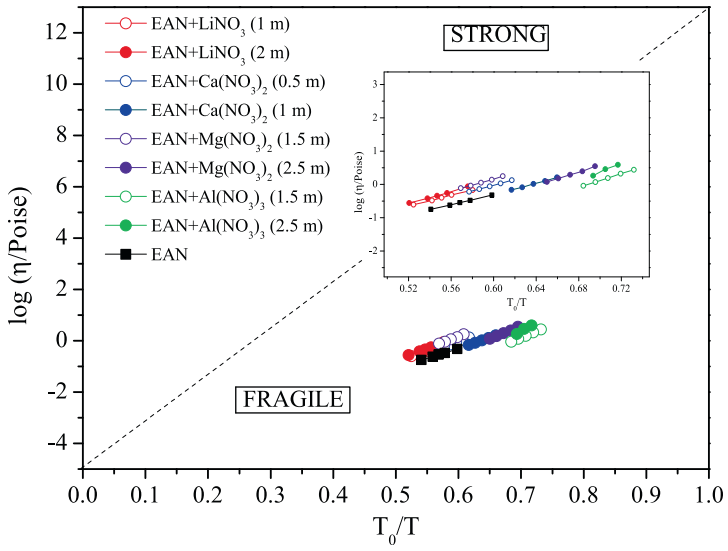

Fig. 12. Fragility plot for pure EAN and its mixtures with $LiNO_3$ (a), $Ca(NO_3)_2$ (b), $Mg(NO_3)_2$ (c) and $Al(NO_3)_3$ (d) near the solubility limit and at an intermediate concentration.

Table 3
Fitting parameters of the experimental conductivities and viscosities of mixtures of EAN with $LiNO_3$, $Mg(NO_3)_2$, $Ca(NO_3)_2$ and $Al(NO_3)_3$ to the Arrhenius equation.

IL	*Conductivity*		*Viscosity*			
	$\ln\sigma_\infty$ (mS cm^{-1})	E_A^Λ (kJ mol^{-1})	$\ln\eta_\infty$ (mPa· s)	E_A^η (kJ mol^{-1})	ζ^{Walden}	$\zeta = E_A^\Lambda/E_A^\eta$
EAN	10.01 ± 0.12	16.89 ± 0.34	-6.42 ± 0.19	24.24 ± 0.43	0.813 ± 0.036	0.70
EAN + LiNO$_3$ (1 m)	$10,20 \pm 0.18$	18.23 ± 0.06	-6.49 ± 0.23	25.20 ± 0.56	0.89 ± 0.03	0.72
EAN + LiNO$_3$ (2 m)	10.78 ± 0.19	20.08 ± 0.06	-7.51 ± 0.37	28.12 ± 0.91	0.85 ± 0.03	0.71
EAN + Ca(NO$_3$)$_2$ (0.5 m)	11.17 ± 0.28	21.32 ± 0.09	-7.43 ± 0.18	29.49 ± 0.45	$1,27 \pm 0.20$	0.72
EAN + Ca(NO$_3$)$_2$ (1 m)	11.65 ± 0.30	22.93 ± 0.10	-8.20 ± 0.33	31.81 ± 0.82	1.28 ± 0.08	0.72
EAN + Mg(NO$_3$)$_2$ (1.5 m)	12.00 ± 0.37	23.96 ± 0.12	-7.50 ± 0.34	30.30 ± 0.83	1.44 ± 0.08	0.79
EAN + Mg(NO$_3$)$_2$ (2.5 m)	12.40 ± 0.21	25.74 ± 0.07	-10.51 ± 0.59	39.1 ± 1.5	1.01 ± 0.06	0.66
EAN + Al(NO$_3$)$_3$ (1.5 m)	12.57 ± 0.35	25.90 ± 0.11	-11.63 ± 0.27	41.31 ± 0.66	1.51 ± 0.24	0.63
EAN + Al(NO$_3$)$_3$ (2.5 m)	13.68 ± 0.40	29.80 ± 0.13	-17.3 ± 2.7	57.7 ± 6.7	0.95 ± 0.04	0.52

reported by Angell and Sare [56]. According to these authors, the formal charge of the cation exerts a significant influence on the glass transition temperature of aqueous electrolyte solutions, together with the viscosity coefficient. However, the same authors warn that this is not the dominant factor determining the value of T_g for an arbitrarily selected electrolyte solution, and that the role of the anion has to be also properly taken into account. The absence of sharp jumps in conductivity in the supercooled region for the studied cations suggests that salt addition confers a stronger character to the ionic mixtures relative to that of pure EAN [57,58].

Fig. 10 presents the Arrhenius plot for the conductivities of the mixtures analyzed in this paper, and Fig. 11 shows the same plot for the viscosities. These compounds clearly exhibit a non-Arrhenius glassy dynamics, since their conductivities increase in a non-linear way with increasing temperature. This glass transition in the low temperature region is related to a slowdown of both relaxation and transport processes [59], which is due to a huge decrease in the number of accessible microstates (configurational entropy) as temperature decreases. As a result, the relaxation and transport mechanisms experience several restrictions that are described by the Vogel-Fulcher-Tammann (VFT) equation [60,61]

$$\ln\sigma = \ln\sigma_\infty - \frac{DT_0}{T - T_0}, \tag{3}$$

where D is the fragility index or strength index, which is inversely proportional to the kinetic fragility of the liquid [62], and T_0 is the vanishing mobility temperature, also known as the Vogel temperature. As it is well-known, these dense ionic systems exhibit, in general, a thermal activation of the VFT type [63,64], which is associated to the presence of several relaxation times in the underlying dynamics characteristic of disordered systems. On the other hand, the Vogel temperature included in Eq. 3 can be considered to essentially agree with the glass transition temperature for infinitely slow processes [65], which is approximately the case in this work. In those cases in which $T \gg T_0$, the previous equation recovers the Arrhenius relation

$$\ln\sigma = \ln\sigma_\infty - \frac{E_A^\Lambda}{k_B T}, \tag{4}$$

when the activation energy of the conductivity, E_A^Λ, is the same for all the ionic hopping motions between ion cages, the main charge transport mechanism in ILs and their mixtures, as has been reported by Araque et al. [66–68]. The experimental values obtained for the conductivities included in Fig. 10 were fitted to the VFT Eq. (3) and the obtained parameters are shown in Table 2. The effective activation energy, which is related to the Vogel temperature and the fragility index by $B = Dk_BT_0$ [9], is also included in Table 2.

As can be observed in Table 2, the conductivity at infinite temperature slightly increases upon the addition of an inorganic salt to the pure IL. Additionally, we found that the Vogel temperature decreases, but for $Ca(NO_3)_2$, as the concentration of the salt increases, which is the opposite trend obtained, in general, for the fragility index. Our results reveal a general behaviour in which

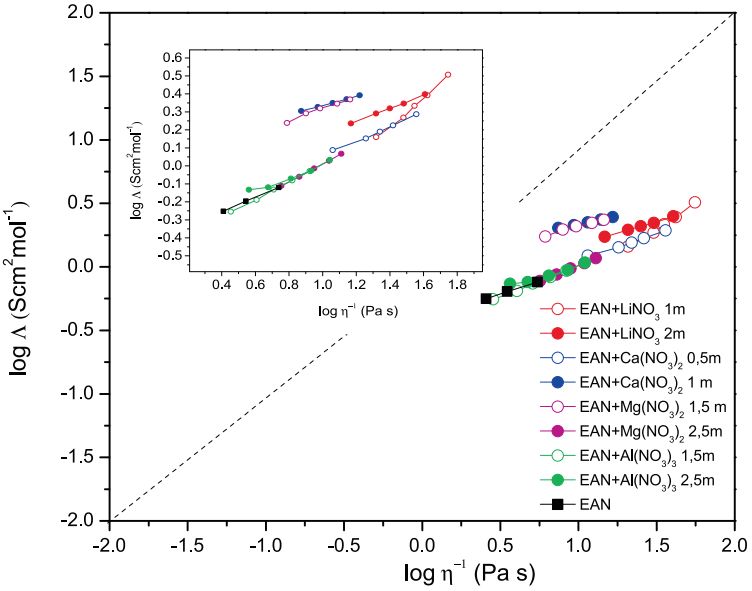

Fig. 13. Walden plot of pure EAN and its mixtures with $LiNO_3$ (a), $Ca(NO_3)_2$ (b), $Mg(NO_3)_2$ (c) and $Al(NO_3)_3$ (d) near the solubility limit and at an intermediate concentration. The lines shown in the plot are guides to the eye. The fitting parameters are included in Table 3.

the mixtures are more fragile the lower the salt cation charge, showing energy landscapes with more potential energy minima and metastable states [57,69,58]. This is also consistent with the inorganic salt breaking a greater fraction of the H-bond network formed in pure EAN the greater the valence of the added salt, hence giving rise to stronger liquids.

Analyzing the fragility plot included in Fig. 12 we can reach the same conclusion. All the mixtures show a behaviour of the viscosity with marked deviations from an Arrhenius law, these deviations being more important the greater the salt cation charge. Since the fragility is a measure of the thermal sensitivity of the liquid, it could be stated that the viscosity of those mixtures with $LiNO_3$ changes in a more gradual way when they are cooled near the glass transition temperature than those systems doped with $Al(NO_3)_3$. That is, the former mixtures "remember" the structure that they had as a glass when they are heated up to the glass transition temperature more strongly than the latter systems do. This behaviour is expected to be related to the lower hydrogen bonding degree of EAN when mixed with inorganic salts with a greater valence.

Finally, we have fitted both the high-temperature conductivity and viscosity data to the Arrhenius equation, and the parameters are shown in Table 3. As can be observed in this table, the limiting conductivities follow the same trend as the one found in the VFT fits. On the other hand, the activation energies increase both with the amount of salt that is present in the mixture and also with the salt cation charge. Furthermore, in Table 3 we compare the activation energies obtained from the fits to Arrhenius equations of the experimental values of both conductivity and viscosity. We can see that the conventional Walden rule ($\Lambda\eta = cte$) does not apply, since both activation energies do not have the same value. Hence, the mechanism of electric conduction by these compounds cannot be considered completely ionic or electrophoretic. In these dense ionic systems, the ions are strongly coordinated and their behaviour deviates from Walden's rule, since conductivity is influenced by inevitable, albeit transient, ion associations and other correlations. In particular, we can observe in Fig. 13 that all the mixtures studied in this work show a subionic behaviour and are located quite far from the ideal line typical of highly diluted, totally dissociated, strong electrolyte solutions represented by the 0.01 M KCl solution. As we have seen, the Walden rule seriously breaks down for this kind of systems and needs to be replaced by the so-called fractional Walden rule, $\Lambda\eta^{\zeta} = C$ [70], where C is a constant known as the Walden product that takes a value between 0 and 1. The fractional Walden rule implies that the Arrhenius activation energy for conductivity is lower than that for viscosity, which can be explained in terms of the different sizes of the ions in ILs. The slope of the fractional Walden plot, ζ, is related to the degree of ionic association and it is expected to be similar to the ratio of the activation energies of conductivity and viscosity. In our case, the ζ values are in good agreement with those obtained by fitting the experimental conductivity and viscosity to the Arrhenius behaviour. Since the Walden plot shows large negative deviations from the ideal line, the presence of very strong correlations (such as ion pairing) must be highlighted. In this case, this indicates once again, in agreement with the evidences shown above, that the doping of the PIL with an inorganic salt leads to the formation of ionic clusters ($[XA_n]^{1-n}$) composed by the cation of the added salt and the anions in the first coordination shell that diffuse as recognizable kinetic entities [22]. To be effective in this respect, these aggregates must be long enough lived so as their lack of contribution to the conduction process becomes important [71], which has been previously proved by some of us [29].

4. Conclusions

In the present paper, we report a systematic analysis of the effect of salt concentration, temperature and cation valence on several equilibrium and transport properties of mixtures of a PIL, EAN, with monovalent ($LiNO_3$), divalent ($Mg(NO_3)_2$, $Ca(NO_3)_2$) and trivalent ($Al(NO_3)_3$) inorganic salts with a common anion. We measured solubility limits of IL-salt mixtures in the presence of residual water, and characterized the state of the water molecules in these media, essential to attain measurable salt solubilities, finding that water molecules are bonded (hydration water) to the highly charged cations (Mg^{2+}, Al^{3+}). Volumetric properties, refractive indices, surface tensions, electric conductivities, and viscosities of the mixtures were then measured. Moreover, fragilities and ionicities of the investigated mixtures have also been a matter of study

by means of the fragility and Walden plots, respectively. The main mechanism of salt solvation was shown to be the formation in the polar nanodomains of the bulk mixture of ionic clusters $[XA_n]^{z-n}$ (mixed $[X(H_2O)_mA_n]^{z-n}$ in case of our presently reported ternary mixtures) of the salt cation with the anions, more strongly bound the higher the surface charge density of the salt cation and arranged into a pseudo-solid pseudolattice. This gives rise to the charge oscillations previously reported in the polar nanoregions of the IL [67,68] as one of the essential structural feature of these densely ionic solvents. Hence, the increase in the salt cation charge was shown to lead to denser and less compressible systems the higher the cation charge, which also produces a larger distortion of the well-known network of H-bonds of the PIL. The refractive indexes generally increase with salt concentration and charge density. The surface tension of the studied mixtures was found to be essentially constant upon salt addition, reflecting a relative indifference of the studied salts to be solvated in the bulk or at the free interface of the IL. On the other hand, transport properties were found to be slowed down with the addition of the inorganic salts, in a more pronounced way for the cations with larger surface charge density (Mg^{2+}, Al^{3+}). Experimental measurements agreed well with MD simulations of the MSDs of the salt cations, which were shown to be trapped in the ionic clusters $[XA_n]^{1-n}$ during longer time intervals the higher their valencies. The effect of the cation charge on the electrical conductivity was tested and shown to be larger the higher the surface charge density of the cation. The cations with the lower surface charge (Li^+, Ca^{2+}) were seen to lead to more mobile systems than the pure solvent in the supercooled region, i.e. at temperatures below the pure EAN melting point, contrarily to its more charged counterparts, indicating that the more weakly bound ionic clusters of cations with low surface charge produce more fragile mixtures. Moreover, the salts with cations of large surface charges give rise to significantly more viscous solutions. The temperature dependence of the conductivity was studied in the Vogel-Fulcher-Tammann (VFT) framework, and we reported fragility indexes, effective activation energies, and Vogel temperatures. All the analyzed mixtures showed to be fragile and subionic systems in the Walden plots, with mixtures of EAN and $Ca(NO_3)_2$ exhibiting the largest fragility. All the reported observations are compatible with the formation of long-lived anionic clusters in the polar regions that act as stable kinetic entities and with a decrease of the hydrogen bonding degree of the PIL when doping pure EAN with an inorganic salt.

CRediT authorship contribution statement

P. Vallet: Investigation, Validation, Formal analysis, Data curation, Visualization. **S. Bouzón-Capelo:** Investigation, Validation, Formal analysis, Data curation, Visualization. **T. Méndez-Morales:** Investigation, Validation, Formal analysis, Data curation, Visualization. Writing (all). **V. Gómez-González:** Investigation, Validation, Formal analysis, Data curation, Visualization. Writing (all). **Y. Arosa:** Investigation, Validation, Formal analysis, Data curation, Visualization. **R. de la Fuente:** Conceptualization, Methodology, Validation, Formal analysis, Investigation, Supervision, Writing (all), Funding acquisition. **E. López Lago:** Conceptualization, Methodology, Validation, Formal analysis, Investigation, Supervision, Writing (all), Funding acquisition. Project administration. **J. R. Rodríguez:** Conceptualization, Methodology, Validation, Formal analysis, Investigation, Supervision, Funding acquisition. **L.J. Gallego:** Conceptualization, Methodology, Validation, Formal analysis, Investigation, Supervision, Writing (review & editing), Funding acquisition. Project administration. **J.J. Parajó:** Investigation, Validation, Formal analysis, Data curation, Visualization. **J. Salgado:** Investigation, Validation, Formal analysis, Data curation, Visualization. Funding acquisition. **M. Turmine:** Investigation, Validation, Formal analysis, Writing (review & editing), Data curation, Visualization. **L. Segade:** Investigation, Validation, Formal analysis, Data curation, Visualization. Funding acquisition. **O. Cabeza:** Conceptualization, Methodology, Software, Validation, Formal analysis, Investigation, Visualization, Writing (all). Funding acquisition. Project administration. **Luis M. Varela:** Conceptualization, Methodology, Validation, Formal analysis, Investigation, Supervision, Writing (all), Funding acquisition. Project administration.

Declaration of Competing Interest

The authors declare that they have no known competing financial interests or personal relationships that could have appeared to influence the work reported in this paper.

Acknowledgement

The financial support of the Spanish Ministry of Economy and Competitiveness (Projects MAT2017-89239-C2-1-P and MAT2017-89239- C2-2-P) is gratefully acknowledged. Moreover, this work was funded by the Xunta de Galicia (ED431D 2017/06, ED431E 2018/08, GRC ED431C 2016/001 and GRC ED431C 2020/10). All these research projects were partially supported by FEDER. P. V. thanks the Spanish Ministry of Science, Innovation and Universities for his FPI grant (PRE2018-084212). T.M.-M. thanks the Spanish Ministry of Science, Innovation and Universities for her Juan de la Cierva grant (IJC2018-036774-I).J. J. Parajó thanks the funding support of I2C postdoctoral program of Xunta de Galicia. Y. A. thanks the funding support from postdoctoral Program of Xunta de Galicia (ED481B-2021-027). Facilities provided by the Galician Supercomputing Centre (CESGA) are also acknowledged.

References

[1] P. Wasserscheid, T. Welton, Ionic Liquids in Synthesis, Wiley Online Library, 2003.
[2] N.V. Plechkova, K.R. Seddon, Ionic Liquids: "Designer" Solvents for Green Chemistry, John Wiley & Sons Inc, 2007, pp. 103–130.
[3] C.A. Angell, N. Byrne, J.-P. Belieres, Parallel Developments in Aprotic and Protic Ionic Liquids: Physical Chemistry and Applications, Acc. Chem. Res. 40 (11) (2007) 1228–1236.
[4] A. Mohammad, Green solvents II. Properties and applications of ionic liquids, Springer, 2012.
[5] K. Ghandi, A Review of Ionic Liquids, Their Limits and Applications, Green Sust. Chem. 4 (1) (2014) 44–53.
[6] R.L. Vekariya, A review of ionic liquids: Applications towards catalytic organic transformations, J. Mol. Liq. 227 (2017) 44–60, https://doi.org/10.1016/j.molliq.2016.11.123, URL: http://www.sciencedirect.com/science/article/pii/S0167732216319432. ISSN 0167-7322.
[7] T.L. Greaves, A. Weerawardena, C.F. Andgre, I. Krodkiewska, C.J. Drummond, Protic Ionic Liquids: Solvents with Tunable Phase Behavior and Physicochemical Properties, J. Phys. Chem. B 110 (45) (2006) 22479–22487.
[8] T.L. Greaves, C.J. Drummond, Protic Ionic Liquids: Properties and Applications, Chem. Rev. 108 (1) (2008) 206–237.
[9] J.-P. Belieres, C.A. Angell, Protic ionic liquids: preparation, characterization, and proton free energy level representation, J. Phys. Chem. B 111 (18) (2007) 4926–4937.
[10] P. Walden, Molecular weights and electrical conductivity of several fused salts, Bull. Russian Acad. Sci. 1914 (1800) 405–422.
[11] A.W.K. Fumino, R. Ludwig, Hydrogen Bonding in Protic Ionic Liquids: Reminiscent of Water, Angew. Chem. Int. Ed. 48 (17) (2009) 3184–3186.
[12] H. Nakamoto, M. Watanabe, Brønsted acid-base ionic liquids for fuel cell electrolytes, Chem. Commun. 24 (2007) 2539–2541.
[13] M. Díaz, A. Ortiz, I. Ortiz, Progress in the use of ionic liquids as electrolyte membranes in fuel cells, J. Membr. Sci. 469 (2014) 379–396.
[14] C. Merlet, B. Rotenberg, P.A. Madden, P.-L. Taberna, P. Simon, Y. Gogotsi, M. Salanne, On the molecular origin of supercapacitance in nanoporous carbon electrodes, Nat. Mater. 11 (2012) 306–310.
[15] Y. Shim, H.J. Kim, Nanoporous Carbon Supercapacitors in an Ionic Liquid: A Computer Simulation Study, ACS Nano 4 (4) (2010) 2345–2355.
[16] Y. Shim, Y. Jung, H.J. Kim, Graphene-Based Supercapacitors: A Computer Simulation Study, J. Phys. Chem. C 115 (47) (2011) 23574–23583.

[17] V. Borgel, E. Markevich, D. Aurbach, G. Semrau, M. Schmidt, On the application of ionic liquids for rechargeable Li batteries: High voltage systems, J. Power Sources 189 (1) (2009) 331–336.
[18] A. Lewandowski, A. Świderska Mocek, Ionic liquids as electrolytes for Li-ion batteries–An overview of electrochemical studies, J. Power Sources 194 (2009) 601–609.
[19] E. Markevich, V. Baranchugov, D. Aurbach, On the possibility of using ionic liquids as electrolyte solutions for rechargeable 5V Li ion batteries, Electrochem. Commun. 8 (8) (2006) 1331–1334.
[20] S. Menne, J. Pires, M. Anouti, A. Balducci, Protic ionic liquids as electrolytes for lithium-ion batteries, Electrochem. Commun. 31 (2013) 39–41.
[21] S. Menne, T. Vogl, A. Balducci, Lithium coordination in protic ionic liquids, Phys. Chem. Chem. Phys. 16 (12) (2014) 5485–5489.
[22] T. Méndez-Morales, J. Carrete, O. Cabeza, O. Russina, A. Triolo, L.J. Gallego, L.M. Varela, Solvation of Lithium Salts in Protic Ionic Liquids: A Molecular Dynamics Study, J. Phys. Chem. B 118 (3) (2014) 761–770.
[23] T. Méndez-Morales, J. Carrete, J.R. Rodríguez, O. Cabeza, L.J. Gallego, O. Russina, L.M. Varela, Nanostructure of mixtures of protic ionic liquids and lithium salts: effect of alkyl chain length, Phys. Chem. Chem. Phys. 17 (7) (2015) 5298–5307.
[24] P. D'Angelo, A. Zitolo, F. Ceccacci, R. Caminiti, G. Aquilanti, Structural characterization of zinc(II) chloride in aqueous solution and in the protic ionic liquid ethyl ammonium nitrate by x-ray absorption spectroscopy, J. Chem. Phys. 135 (15) (2011), 154509(1)–154509(7).
[25] T. Vogl, S. Menne, R.S. Kühnel, A. Balducci, The beneficial effect of protic ionic liquids on the lithium environment in electrolytes for battery applications, J. Mater. Chem. A 2 (22) (2014) 8258–8265.
[26] T. Vogl, S. Menne, A. Balducci, Mixtures of protic ionic liquids and propylene carbonate as advanced electrolytes for lithium-ion batteries, Phys. Chem. Chem. Phys. 16 (45) (2014) 25014–25023.
[27] V. Gómez-González, B. Docampo-Álvarez, O. Cabeza, M. Fedorov, R.M. Lynden-Bell, L.J. Gallego, L.M. Varela, Molecular dynamics simulations of the structure and single-particle dynamics of mixtures of divalent salts and ionic liquids, J. Chem. Phys. 143 (12) (2015) 124507.
[28] P. Ray, T. Vogl, A. Balducci, B. Kirchner, Structural Investigations on Lithium-Doped Protic and Aprotic Ionic Liquids, J. Phys. Chem. B 121 (20) (2017) 5279–5292.
[29] T. Méndez-Morales, J. Carrete, S. Bouzón-Capelo, M. Pérez-Rodríguez, O. Cabeza, L.J. Gallego, L.M. Varela, MD Simulations of the Formation of Stable Clusters in Mixtures of Alkaline Salts and Imidazolium-Based Ionic Liquids, J. Phys. Chem. B 117 (11) (2013) 3207–3220.
[30] O. Russina, R. Caminiti, T. Méndez-Morales, J. Carrete, O. Cabeza, L. Gallego, L. Varela, A. Triolo, How does lithium nitrate dissolve in a protic ionic liquid?, J Mol. Liq. 205 (2015) 16–21.
[31] R. Hayes, S.A. Bernard, S. Imberti, G.G. Warr, R. Atkin, Solvation of Inorganic Nitrate Salts in Protic Ionic Liquids, J. Phys. Chem. C 118 (36) (2014) 21215–21225.
[32] L. Niedzicki, E. Karpierz, M. Zawadzki, M. Dranka, M. Kasprzyk, A. Zalewska, M. Marcinek, J. Zachara, U. Domańska, W. Wieczorek, Lithium cation conducting TDI anion-based ionic liquids, Phys. Chem. Chem. Phys. 16 (23) (2014) 11417–11425.
[33] E. Karpierz, L. Niedzicki, T. Trzeciak, M. Zawadzki, M. Dranka, J. Zachara, G. Żukowska, A. Bitner-Michalska, W. Wieczorek, Ternary mixtures of ionic liquids for better salt solubility, conductivity and cation transference number improvement, Sci. Rep. 6 (2016) 35587.
[34] Z. Li, O. Borodin, G.D. Smith, D. Bedrov, Effect of Organic Solvents on Li+ Ion Solvation and Transport in Ionic Liquid Electrolytes: A Molecular Dynamics Simulation Study, J. Phys. Chem. B 119 (7) (2015) 3085–3096.
[35] J. Vila, P. Gines, E. Rilo, O. Cabeza, L. Varela, Great increase of the electrical conductivity of ionic liquids in aqueous solutions, Fluid Ph. Equilibria. 247 (1) (2006) 32–39.
[36] L. Suo, O. Borodin, T. Gao, M. Olguin, J. Ho, X. Fan, C. Luo, C. Wang, K. Xu, "Water-in-salt" electrolyte enables high-voltage aqueous lithium-ion chemistries, Science 350 (6263) (2015) 938–943.
[37] J.O. Besenhard, M. Winter, Advances in Battery Technology: Rechargeable Magnesium Batteries and Novel Negative-Electrode Materials for Lithium Ion Batteries, Chem. Phys. Chem. 3 (2) (2002) 155–159.
[38] O. Mizrahi, N. Amir, E. Pollak, O. Chusid, V. Marks, H. Gottlieb, L. Larush, E. Zinigrad, D. Aurbach, Electrolyte Solutions with a Wide Electrochemical Window for Rechargeable Magnesium Batteries, J. Electrochem. Soc. 155 (2) (2008) A103–A109.
[39] Z. Chen, T.L. Greaves, C. Fong, R.A. Caruso, C.J. Drummond, Lyotropic liquid crystalline phase behaviour in amphiphile–protic ionic liquid systems, Phys. Chem. Chem. Phys. 14 (11) (2012) 3825–3836.
[40] R.D. Shannon, Revised effective ionic radii and systematic studies of interatomic distances in halides and chalcogenides, Acta Crystallogr. Sect. A 32 (5) (1976) 751–767.
[41] M.A. Cabrerizo-Vílchez, H.A. Wege, J.A. Holgado-Terriza, A.W. Neumann, Axisymmetric drop shape analysis as penetration Langmuir balance, Rev. Sci. Instrum. 70 (5) (1999) 2438–2444.
[42] Y. Arosa, E. López-Lago, L.M. Varela, R. de la Fuente, Spectrally resolved white light interferometry to measure material dispersion over a wide spectral band in a single acquisition, Opt. Express 24 (15) (2016) 17303–17312.
[43] Y. Arosa, E. López-Lago, R. de la Fuente, Refractive index retrieval in the UV range using white light spectral interferometry, Opt. Mater. 82 (2018) 88–92.
[44] Y. Arosa, E. López-Lago, R. de la Fuente, Spectrally resolved white light interferometer for measuring dispersion in the visible and near infrared range, Measurement 122 (2018) 6–13.
[45] D.V.D. Spoel, E. Lindahl, B. Hess, A.R.V. Buuren, E. Apol, P.J. Meulenhoff, D.P. Tieleman, A.L.T.M. Sijbers, K.A. Feenstra, R.V. Drunen, H.J.C. Berendsen, Gromacs User Manual version 4.0, http://www.Gromacs.org, 2005.
[46] W.L. Jorgensen, Optimized Intermolecular Potential Functions for Liquid Alcohols, J. Phys. Chem. 90 (7) (1986) 1276–1284.
[47] Y. Umebayashi, W.-L. Chung, T. Mitsugi, S. Fukuda, M. Takeuchi, K. Fujii, T. Takamuku, R. Kanzaki, S. Ishiguro, Liquid Structure and the Ion-Ion Interactions of Ethylammonium Nitrate Ionic Liquid Studied by Large Angle X-Ray Scattering and Molecular Dynamics Simulations, J. Comput. Chem. Jpn. 7 (4) (2008) 125–134.
[48] J. Choe, K. Kim, S. Chang, Computer Simulations on Molecular Recognition of Alkylamines by Ester Derivatives of p-tert-butylcalix[6]arene, Bull. Korean Chem. Soc. 21 (2) (2000) 200–206.
[49] S.V. Sambasivarao, O. Acevedo, Development of OPLS-AA Force Field Parameters for 68 Unique Ionic Liquids, J. Chem. Theory Comput. 5 (4) (2009) 1038–1050.
[50] A.P. Lyubartsev, K. Laasonen, A. Laaksonen, Hydration of Li+ ion. An ab initio molecular dynamics simulation, J. Chem. Phys. 114 (7) (2001) 3120–3126.
[51] V. Gómez-González, B. Docampo-Álvarez, O. Cabeza, M. Fedorov, R.M. Lynden-Bell, L.J. Gallego, L.M. Varela, Molecular dynamics simulations of the structure and single-particle dynamics of mixtures of divalent salts and ionic liquids, J. Chem. Phys. 143 (12) (2015) 124507.
[52] N. Laberge, V. Vasilescu, C. Montrose, P. Macedo, Equilibrium compressibilities and density fluctuations in K_2O-SiO_2 glasses, J. Am. Ceram. Soc. 56 (10) (1973) 506–509.
[53] S.B. Capelo, T. Méndez-Morales, J. Carrete, E. López-Lago, J. Vila, O.C.J.R. Rodríguez, M. Turmine, L.M. Varela, Effect of Temperature and Cationic Chain Length on the Physical Properties of Ammonium Nitrate-Based Protic Ionic Liquids, J. Phys. Chem. B 116 (36) (2012) 11302–11312.
[54] L. Segade, M. Cabanas, M. Domínguez-Pérez, E. Rilo, S. García-Garabal, M. Turmine, L.M. Varela, V. Gómez-González, B. Docampo-Alvarez, O. Cabeza, Surface and bulk characterisation of mixtures containing alkylammonium nitrates and water or ethanol: Experimental and simulated properties at 298.15 K, J. Mol. Liq. 222 (2016) 663–670.
[55] M. Hoorfar, M.A. Kurz, Z. Policova, M.L. Hair, A.W. Neumann, Do polysaccharides such as dextran and their monomers really increase the surface tension of water?, Langmuir 22 (1) (2006) 52–56
[56] C.A. Angell, E. Sare, Glass-Forming Composition Regions and Glass Transition Temperatures for Aqueous Electrolyte Solutions, J. Chem. Phys. 52 (3) (1970) 1058–1068.
[57] C. Angell, Relaxation in liquids, polymers and plastic crystals -strong/fragile patterns and problems, J. Non-Cryst. Solids 131 (1991) 13–31, ISSN 0022-3093, proceedings of the International Discussion Meeting on Relaxations in Complex Systems.
[58] S. Sastry, The relationship between fragility, configurational entropy and the potential energy landscape of glass-forming liquids, Nature 409 (6817) (2001) 164–167.
[59] T. Kitamura, Quantum field theory of the liquid-glass transition, Phys. Rep. 383 (1) (2003) 1–94.
[60] H. Vogel, The law of the relation between the viscosity of liquids and the temperature, Phys. Z 22 (1921) 645–646.
[61] G. Tammann, W. Hesse, Die Abhängigkeit der Viscosität von der Temperatur bie unterkühlten Flüssigkeiten, Anorg. Allg. Chem. 156 (1) (1926) 245–257.
[62] R. Böhmer, K.L. Ngai, C.A. Angell, D.J. Plazek, Nonexponential relaxations in strong and fragile glass formers, J. Chem. Phys. 99 (5) (1993) 4201–4209.
[63] J. Vila, P. Ginés, J.M. Pico, C. Franjo, E. Jiménez, L.M. Varela, O. Cabeza, Temperature dependence of the electrical conductivity in EMIM-based ionic liquids: Evidence of Vogel–Tamman–Fulcher behavior, Fluid Ph. Equilibria. 242 (2) (2006) 141–146.
[64] J. Vila, C. Franjo, J.M. Pico, L.M. Varela, O. Cabeza, Temperature Behavior of the Electrical Conductivity of Emim-Based Ionic Liquids in Liquid and Solid States, Port. Electrochim. Acta 25 (1) (2007) 163–172.
[65] L.M. Martinez, C.A. Angell, A thermodynamic connection to the fragility of glass-forming liquids, Nature (London) 410 (2001) 663–667.
[66] L.M. Varela, J. Carrete, M. García, L.J. Gallego, M. Turmine, E. Rilo, O. Cabeza, Pseudolattice theory of charge transport in ionic solutions: Corresponding states law for the electric conductivity, Fluid Phase Equil. 298 (2010) 280.
[67] J.C. Araque, S.K. Yadav, M. Shadeck, M. Maroncelli, C.J. Margulis, How is diffusion of neutral and charged tracers related to the structure and dynamics of a room-temperature ionic liquid? Large deviations from Stokes-Einstein behavior explained, J. Phys. Chem. B 119 (23) (2015) 7015–7029.
[68] J.C. Araque, J.J. Hettige, C.J. Margulis, Modern room temperature ionic liquids, a simple guide to understanding their structure and how it may relate to dynamics, J. Phys. Chem. B 119 (40) (2015) 12727–12740.
[69] P.G. Debenedetti, F.H. Stillinger, Supercooled liquids and the glass transition, Nature 410 (2001) 259–267.
[70] W. Xu, C.A. Angell, Solvent-free electrolytes with aqueous solution-like conductivities, Science 302 (5644) (2003) 422–425.
[71] D.R. MacFarlane, M. Forsyth, E.I. Izgorodina, A.P. Abbott, G. Annat, K. Fraser, On the concept of ionicity in ionic liquids, Phys. Chem. Chem. Phys. 11 (25) (2009) 4962–4967.